The Level Set Method for Simulating Gravity Currents

by

Nathan Braniff

A research report
presented to the University of Waterloo
in fulfillment of the
research requirement for the degree of
Master of Mathematics
in
Computational Mathematics

Waterloo, Ontario, Canada, 2016

I hereby declare that I am the sole author of this work. This is a true copy of the work, including any required final revisions, as accepted by my examiners.

I understand that my thesis may be made electronically available to the public.

Abstract

Gravity currents are a type of two-phase fluid flow driven by density differences between two immiscible fluids. They appear in a large number of natural and industrial phenomena and have been, and continue to be, of mathematical interest.

In this work we investigate a gravity flow resulting from a dam break problem, as a slightly denser fluid subducts under a less dense one. In order to numerically simulate these flows, an accurate and efficient methodology is required to track the fluid interface. We develop a numerical algorithm to solve the Navier Stokes equations for incompressible two-phase flows, in conjunction with the Level Set Method to track the interface between the two fluids with differing densities. We assess the asymptotic behaviour of our numerical simulation at high Reynolds numbers and long simulation times against previous numerical work on inviscid flows. While the computational efficiency of the algorithm has proved to be a bottleneck, we achieve good agreement with regards to the speed of the flow front calculated in past works.

Acknowledgements

I would like to thank my supervisors, Serge D'Alessio and Justin Wan, for their careful attention and support, without whom this work would not be possible. I would also like to thank my classmates in the Computational Math program for their generosity and friendship.

Dedication

This work is dedicated to my family for their unwavering support.

Table of Contents

List of Tables

List of Figures

Chapter 1

Introduction

In this work we investigate the propagation of a two-phase gravity flow resulting from a dam break in two dimensions. Gravity flows are formed when two immiscible fluids of differing densities are contained in the same domain. Gravity, acting in the vertical direction, and the differing densities cause one fluid to flow over or under the other fluid, with propagation occurring mostly in the horizontal direction. Gravity currents appear in a range of natural phenomenon including behaviour observed in the atmosphere and ocean [12]. One of the defining features of a gravity current is that the vertical length scale is much smaller than the horizontal length, with the current resulting in long thin flows in the horizontal direction. Analytic work often makes use of this when constructing approximations [2].

Our specific problem will focus on a dam break scenario between two nearly identical fluids. A slightly denser fluid contained within a rectangular domain against a solid vertical boundary at the left side of the domain will be released instantaneously. Our simulation will observe its propagation as it subducts under a less dense fluid and propagates across the bottom of the domain. Figure 1.1 shows an illustration of the initial conditions. We are specifically addressing the problem where there is no stiff boundary at the top or right side of the domain.

1.1 Gravity Currents

Original analytic investigation of the dam break problem started with Saint-Venant [4]. However, the first theoretical study of gravity currents is often attributed to von Karman in

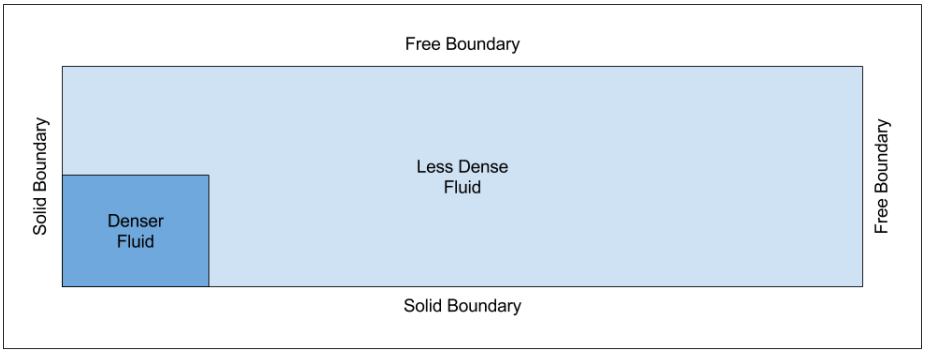

Figure 1.1: *A depiction of the initial conditions for the domain of the simulated gravity current problem.*

1940 [30], who addressed the propagation speed of a denser fluid flowing under a less dense one. Early experimental results were also achieved by Keulegan [17, 18] and Middleton [21]. The earliest numerical experiments come from Daly and Pracht [3], who achieved good concordance with experimental data. These early simulations used marker tracking techniques to handle the fluid interface, unlike the level set technique which is used here. A number of early modeling attempts by Benjamin [1] and Huppert [13] used simplified formulations to achieve some general agreement with experimental results. Rottman and Simpson [24] as well as Kao et al. [16] have investigated the propagation of currents under fixed upper boundaries. Much of this work focuses on high-Reynolds number or inviscid flows. Since then a number of review papers have been published [12, 6, 9] along with two comprehensive texts [28, 26]. Figure 1.2 contains an image of an experimental gravity current as it propagates.

In this work we have solved a finite difference approximation for the gravity current problem. We use this to simulate the gravity current with outflow boundary conditions on the top and far wall of the domain. These conditions approximate the domain continuing in these directions. Earlier numerical solutions to this problem exist for the inviscid case. D'Alessio et al. [2] have investigated the gravity current propagation for the dam break problem in a rectangular channel which has a free boundary at the top of the domain. Their work solves the problem for the inviscid case and therefore our solution is hypothesized to approaches theirs at large Reynolds numbers. In this work we attempt to understand the asymptotic behaviour of our more general finite difference solution as it approaches the inviscid results at high Reynolds numbers.

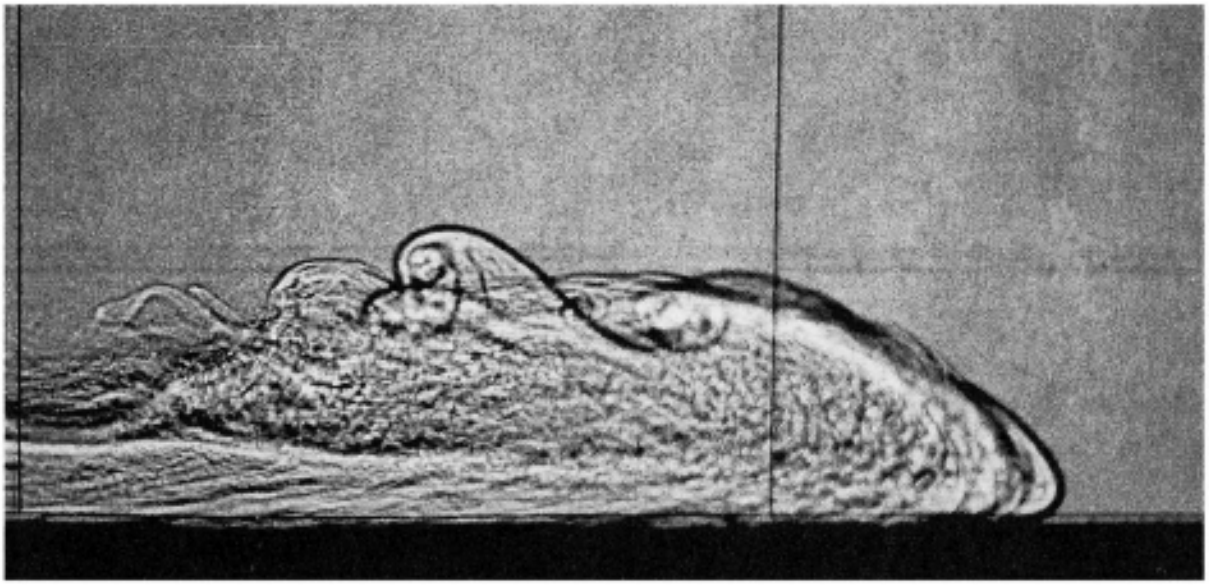

Figure 1.2: *A shadowgraph of an experimental gravity current, mid flow [26].*

1.2 Simulating the Fluid Interface

As the gravity current problem involves a two-phase flow, it requires some methodology for localizing the fluid interface. This can be accomplished in a number of different ways. There are two main categories for implementing the fluid boundary: interface tracking methods that explicitly track the interface location, and interface capturing methods which use a separate scalar function defined over the domain, from which the boundary can be computed [20].

Interface tracking methods consist of schemes such as front tracking or marker tracking methods which generally use specific markers, which are placed along the fluid interface [14]. By tracking these markers through time, the interface can be localized. The resolution with which the interface location can be determined is dependent on the number of markers. Thus higher resolution requires an increased computational cost [20].

The second set of methods involve interface capturing methods. An example of these methods is the Volume of Fluid method [20]. In this method a scalar function ranging from 0 to 1 is defined for each parcel of the domain and its value indicates how much of each fluid is present within it. The interface is therefore denoted by cells with a fractional

value [20]. However, in our work we utilize the level set method [23, 25]. In this approach a scalar function is defined across the domain, and its zero level set is treated as the fluid interface. By advecting this function with the appropriate velocity field, the zeroth level set, and thus the interface, move accordingly. A similar discretization and implementation of the level set method can be found in the work of Fattori [5].

Chapter 2

Governing Equations and Mathematical Formulation

In the following chapter we will introduce the governing equations of motion and the mathematical machinery used to capture the fluid interface for the gravity current problem in two dimensions. We will first discuss the derivation of the specific formulation of the Navier Stokes equations used. We will then discuss the interface conditions used along the fluid interface and the boundary conditions along the edges of the domain. Finally, we will discuss the localization of the interface using the level set method and the propagation of the level set function in time.

2.1 Navier-Stokes Equations for Incompressible Flow

We begin with Navier-Stokes equations in two dimensions for incompressible flows. These consist of two momentum equations, one for each direction and the continuity equation, all of which are shown here in dimensional form [8];

Momentum equations:

$$\frac{\partial u}{\partial t} = \frac{\mu}{\rho}\Big(\frac{\partial^2 u}{\partial x^2} + \frac{\partial^2 u}{\partial y^2}\Big) - \frac{\partial u^2}{\partial x} - \frac{\partial uv}{\partial y} - \frac{1}{\rho}\frac{\partial p}{\partial x}, \tag{2.1}$$

$$\frac{\partial v}{\partial t} = \frac{\mu}{\rho}\Big(\frac{\partial^2 v}{\partial x^2} + \frac{\partial^2 v}{\partial y^2}\Big) - \frac{\partial v^2}{\partial y} - \frac{\partial uv}{\partial x} - \frac{1}{\rho}\frac{\partial p}{\partial y} - g, \tag{2.2}$$

Continuity equation:

$$0 = \frac{\partial u}{\partial x} + \frac{\partial v}{\partial y}. \tag{2.3}$$

In the above equations ρ is the fluid density, which is constant within each fluid due to incompressibility. The value μ is the dynamic viscosity of the fluid, also a constant within each fluid. The term g is the gravitational constant and u and v are the velocities in the horizontal and vertical directions respectively.

These equations can be put in dimensionless form by scaling each of the variables according to the following transformations;

$$u^* = \frac{u}{U_\infty}, \quad v^* = \frac{v}{\delta U_\infty}, \quad x^* = \frac{x}{L}, \quad y^* = \frac{y}{H}, \quad p^* = \frac{p}{\rho U_\infty^2}, \quad t^* = \frac{t U_\infty}{L}, \tag{2.4}$$

where,

$$U_\infty = \sqrt{g' H}, \ \delta = \frac{H}{L} << 1. \tag{2.5}$$

The starred terms are the new, dimensionless, quantities scaled by their characteristic scaling factors. Here H and L are the characteristic height and length scale for the problem. The δ term represents the ratio of the characteristic scale height to the scale length and, for the gravity current problem, this value is much less than one. The U_∞ term is the surface gravity wave speed.

Using the above relations we can reexpress the original Navier-Stokes equations in the dimensionless form. We omit the starred notation for convenience here and from this point onward;

$$\delta \frac{\partial u}{\partial t} = \frac{\delta^2}{Re}\frac{\partial^2 u}{\partial x^2} + \frac{1}{Re}\frac{\partial^2 u}{\partial y^2} - \delta \frac{\partial u^2}{\partial x} - \delta \frac{\partial uv}{\partial y} - \delta \frac{\partial p}{\partial x}, \tag{2.6}$$

$$\delta^2 \frac{\partial v}{\partial t} = \frac{\delta^3}{Re}\frac{\partial^2 v}{\partial x^2} + \frac{\delta}{Re}\frac{\partial^2 v}{\partial y^2} - \delta^2 \frac{\partial v^2}{\partial y} - \delta^2 \frac{\partial uv}{\partial x} - \delta \frac{\partial p}{\partial y} - \frac{g}{g'}, \tag{2.7}$$

$$0 = \frac{\partial u}{\partial x} + \frac{\partial v}{\partial y}. \tag{2.8}$$

Above, Re is the Reynolds number for a given fluid defined as $Re = \frac{\rho U_\infty L}{\mu}$. Furthermore, as we have two fluids with different densities, and therefore different gravitational constants per unit volume, we will recast the gravitational constant as well. The new gravitational

constant will be expressed as the ratio of the original gravitational constant to the reduced gravity, g' [2];

$$\frac{g}{g'} = \frac{\rho_1}{\rho_1 - \rho_2}. \tag{2.9}$$

The dimensionless form of the equations hold within each fluid, however, as previously stated, for the gravity current problem there are two different fluids each with potentially different densities and viscosities. This introduces complexity along their interface and necessitates the derivation of interface conditions so that perpendicular and tangential stresses are handled appropriately where the fluids meet [22]. The pressure along the fluid interface is related by the following approximate interface condition according to Nepomnyashchy [22];

$$\rho_1(p_1 + \Delta p) = \rho_2 p_2. \tag{2.10}$$

This condition implies that the pressure within one fluid on the interface is linearly related to the pressure within the other fluid on the other side by the densities of the two fluids and an additive constant Δp which is due to the surface tension. Here p_1 and ρ_1 belong to the first fluid and p_2 and ρ_2 belong to the second.

In these experiments we have neglected surface tension along the interface and thus the Δp term. This is justified due to the magnitude of the Bond number, which measures the effect of surface tension relative to other forces [11]. A Bond number much larger than unity indicates that surface tension has little effect on the problem. The Bond number is defined as follows;

$$B = \frac{\rho g' L^2}{\gamma}, \tag{2.11}$$

where,

$$g' = \Big(\frac{\Delta p}{\rho}\Big) g. \tag{2.12}$$

Here we observed that for two fluids with properties very similar to water and slightly different densities the Bond number must be much greater than one.

Now we derive an interface condition for the tangential stress, which will relate the fluid velocities on each side of the interface. Similar work can be found in Kang et al. [15], however we use the approximation from Huppert[11], where we have the following;

$$\frac{\partial u_1}{\partial y} + \delta^2 \frac{\partial v_1}{\partial x} - 4\delta^2 h_x \frac{\partial u_1}{\partial x} = \frac{\mu_2}{\mu_1} \frac{\partial u_2}{\partial y}. \tag{2.13}$$

Where h_x is the derivative of the interface height with respect to x. relations are derived in the work of Kang et al. [15]. Due to δ being very small we can disregard the second two terms on the left side. This results in the following simpler interface condition in the vertical direction shown here;

$$\mu_1 \frac{\partial u_1}{\partial y} = \mu_2 \frac{\partial u_2}{\partial y}. \tag{2.14}$$

This condition implies that the change of the horizontal velocity around the interface in the vertical direction must be proportional within each fluid, as a function of the ratio of the fluid viscosities.

The above interface condition applies to horizontal velocity but similar conditions are required in both the horizontal direction and the V velocity field. We generalize the above condition to those cases as an approximation, and in lieu of other physical constraints;

$$\mu_1 \frac{\partial u_1}{\partial y} = \mu_2 \frac{\partial u_2}{\partial y}, \quad \mu_1 \frac{\partial u_1}{\partial x} = \mu_2 \frac{\partial u_2}{\partial x}, \tag{2.15}$$

$$\mu_1 \frac{\partial v_1}{\partial y} = \mu_2 \frac{\partial v_2}{\partial y}, \quad \mu_1 \frac{\partial v_1}{\partial x} = \mu_2 \frac{\partial v_2}{\partial x}. \tag{2.16}$$

2.2 Initial and Boundary Conditions

In order to implement the above discretizations we must implement the boundary conditions for the velocity fields, the pressure and the level set function. We begin with the velocity fields; from the gravity current problem definition we require that we have solid, frictionless barriers along the left and bottom sides of the domain. Therefore the velocities perpendicular to these boundaries must be zero due to the impermeability condition, and a free-slip condition is applied along the left and bottom sides due to the lack of friction. To implement both of these we require that the following conditions hold;

Bottom boundary:

$$v = 0, \quad \frac{\partial u}{\partial y} = 0, \tag{2.17}$$

Left boundary:

$$u = 0, \quad \frac{\partial v}{\partial x} = 0. \tag{2.18}$$

The top and right boundaries will impose a free-slip condition on the velocity field moving parallel to the boundary and an outflow condition on the field moving perpendicular to them. This is to reduce the effect of a solid boundary and approximate the domain continuing in the these directions. To enforce these conditions we have the following constraints;

Top boundary:

$$\frac{\partial u}{\partial y} = 0, \quad \frac{\partial v}{\partial y} = 0, \tag{2.19}$$

Right boundary:

$$\frac{\partial v}{\partial x} = 0, \quad \frac{\partial u}{\partial x} = 0. \tag{2.20}$$

For the pressure solver we impose Neumann type boundary conditions. With no true physical constraints to impose on the pressure boundary, the Neumann condition is a neutral choice [8];

Left and right boundaries:

$$\frac{\partial p}{\partial x} = 0, \tag{2.21}$$

Top and bottom boundaries:

$$\frac{\partial p}{\partial y} = 0. \tag{2.22}$$

2.3 Interface Equation

In order to capture the fluid interface, we apply the level set method [23, 25]. Using this method we will represent the fluid boundary as the zero level set of a function defined across the whole domain. We will refer to this level set function as $\phi(x, y)$; or ϕ as a shorthand. Furthermore, the points where ϕ takes a negative value will be considered as part of the denser fluid and the positive points will consist of the second, less dense, fluid:

$$Fluid\ Interface : \{\ (x, y)\ |\ \phi(x, y) = 0\}. \tag{2.23}$$

We can choose any level set function whose zero level set traces the correct interface location for our problem's initial conditions. We will leave discussion of the initialization of the function until the next chapter, however some level set functions, especially those that are well behaved and that have a slope of approximately unity near the interface, are more desirable from a numerical standpoint.

Once the level set function is defined, it is necessary to specify how it should be moved with respect to the surrounding fluid velocities. In order to accomplish this we can use the level set equation [23];

$$\phi_t + \vec{u}|\nabla\phi| = 0. \tag{2.24}$$

Here $\vec{u}$ is the, potentially variable, velocity vector which will advect the level set function. The reader will likely recognize that this is a simple advection equation in two dimensions. We can therefore use the velocity field computed at each time step to propagate the level set function, after which the new location of the zero level set will indicate the updated location of the fluid interface.

The level set function needs appropriate boundary conditions to enforce realistic physical interaction between the interface and the boundaries. We enforce Neumann boundary conditions along all boundaries;

Left and right boundary:

$$\frac{\partial\phi}{\partial x} = 0, \tag{2.25}$$

Top and bottom boundary:

$$\frac{\partial\phi}{\partial y} = 0. \tag{2.26}$$

Chapter 3

Algorithm and Numerical Methods

In the previous chapter, the governing equations for the gravity current problem were outlined. This chapter will discuss the implementation of the discretization and numerical algorithm used to solve them. We restate the governing equations here;

$$\delta\frac{\partial u}{\partial t} = \frac{\delta^2}{Re}\frac{\partial^2 u}{\partial x^2} + \frac{1}{Re}\frac{\partial^2 u}{\partial y^2} - \delta\frac{\partial u^2}{\partial x} - \delta\frac{\partial uv}{\partial y} - \delta\frac{1}{\rho}\frac{\partial \hat{p}}{\partial x}, \tag{3.1}$$

$$\delta^2\frac{\partial v}{\partial t} = \frac{\delta^3}{Re}\frac{\partial^2 v}{\partial x^2} + \frac{\delta}{Re}\frac{\partial^2 v}{\partial y^2} - \delta^2\frac{\partial v^2}{\partial y} - \delta^2\frac{\partial uv}{\partial x} - \delta\frac{1}{\rho}\frac{\partial \hat{p}}{\partial y} - \frac{g}{g'}, \tag{3.2}$$

$$0 = \frac{\partial u}{\partial x} + \frac{\partial v}{\partial y}. \tag{3.3}$$

The reader will observe that we have made one alteration to the above equations with respect to the $\frac{\partial p}{\partial y}$ and $\frac{\partial p}{\partial x}$ terms. When these terms were originally nondimensionalized the pressure p was scaled by the density ρ to produce p^*. Thus the nondimensional terms $\frac{\partial p^*}{\partial y}$ and $\frac{\partial p^*}{\partial x}$ contained a dependence on ρ. When we deal with two fluids however, this density constant will vary, and therefore, we recast the equations without the scaling pressure by ρ to be more explicit by using $\hat{p}$ instead, which has the following relation to the other terms;

$$p^* = \frac{p}{\rho U_\infty^2} = \frac{1}{\rho}\hat{p} \tag{3.4}$$

3.1 Discretization of the Domain

The computational domain is discretized into equal sized cells, forming a grid. We use a staggered grid for our discretization. Figure 3.1 depicts the locations at which the computation of the velocity and pressure values are centred within the grid. Pressure values are computed at the cell centres, horizontal velocity values, U, are computed at the centre of the left and right boundaries of each cell and vertical velocities, V, are computed at the center of the top and bottom boundaries. Linear interpolation is used throughout the algorithm to approximate values between computed locations. Indexing is assigned to the pressure cell locations starting at 1 and continuing to i_{max} and j_{max} respectively. The value $u_{i,j}$ is located on the right edge of the cell containing $\hat{p}_{i,j}$ and $v_{i,j}$ is located at the upper edge of the same cell.

Due to the staggered locations, $\hat{P}$ is not defined at the exact domain boundary and U and V are only defined along two of the four edges. We use ghost cells outside of the fluid domain to enforce boundary conditions in these cases. Thus ghost cells are incorporated on all boundaries for the pressure grid. The horizontal velocity grid, U has ghost points along the upper and lower boundary, where the vertical velocity grid, V has ghost points along the left and right boundaries.

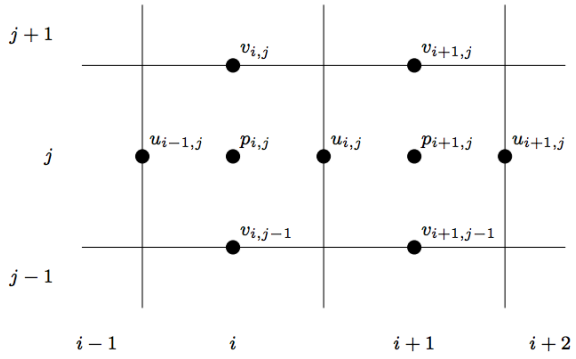

Figure 3.1: *A diagram of a section of the discretized domain, with the location of computed velocity and pressure values [8].*

3.2 Discretization Overview

We will now give a brief overview of the discretization method. We will detail it for a single fluid in the following sections and discuss special considerations for those cells along the fluid interface later on. We begin by explicitly discretizing the time derivatives of U and V within the momentum equations, using forward differencing, to derive a discrete approximation for U and V at the $(n+1)$ time step given the velocities at time n;

$$u^{n+1} = u^n + \frac{\Delta t}{\delta}\Big(\frac{\delta^2}{Re}\frac{\partial^2 u}{\partial x^2} + \frac{1}{Re}\frac{\partial^2 u}{\partial y^2} - \delta\frac{\partial u^2}{\partial x} - \delta\frac{\partial uv}{\partial y} - \frac{\delta}{\rho}\frac{\partial \hat{p}}{\partial x}\Big), \tag{3.5}$$

$$v^{n+1} = v^n + \frac{\Delta t}{\delta^2}\Big(\frac{\delta^3}{Re}\frac{\partial^2 v}{\partial x^2} + \frac{\delta}{Re}\frac{\partial^2 v}{\partial y^2} - \delta^2\frac{\partial v^2}{\partial x} - \delta^2\frac{\partial uv}{\partial y} - \frac{1}{\rho}\frac{\partial \hat{p}}{\partial y} - \frac{g}{g'}\Big). \tag{3.6}$$

To simplify the computation we can rewrite the equations in the following form [8].

$$u^{n+1} = \frac{F^n}{\delta} - \frac{\Delta t}{\rho}\frac{\partial \hat{p}}{\partial x}, \tag{3.7}$$

$$v^{n+1} = \frac{1}{\delta^2}\Big(G^n - \frac{\Delta t}{\rho}\frac{\partial \hat{p}}{\partial y}\Big), \tag{3.8}$$

where F and G are defined as follows;

$$F^n = \delta u^n + \Delta t\Big(\frac{\delta^2}{Re}\frac{\partial^2 u}{\partial x^2} + \frac{1}{Re}\frac{\partial^2 u}{\partial y^2} - \delta\frac{\partial u^2}{\partial x} - \delta\frac{\partial uv}{\partial y}\Big), \tag{3.9}$$

$$G^n = \delta^2 v^n + \Delta t\Big(\frac{\delta^3}{Re}\frac{\partial^2 v}{\partial x^2} + \frac{\delta}{Re}\frac{\partial^2 v}{\partial y^2} - \delta^2\frac{\partial v^2}{\partial y} - \delta^2\frac{\partial uv}{\partial x} - \frac{g}{g'}\Big). \tag{3.10}$$

The F and G terms will be computed at the nth time step whereas the pressure derivative will be computed for the $(n+1)$ timestep [8]. Thus the discretized momentum equations are explicit with respect to velocity but implicit with respect to pressure. The F and G terms will be approximated at the same locations in the grid as U and V are, respectively. Substituting the above into the continuity equation evaluated at time $(n+1)$, we can derive a relation for pressure;

$$0 = \frac{\partial u^{n+1}}{\partial x} + \frac{\partial v^{n+1}}{\partial y} = \frac{1}{\delta}\frac{\partial F^n}{\partial x} - \frac{\Delta t}{\rho}\frac{\partial^2 \hat{p}}{\partial x^2} + \frac{1}{\delta^2}\Big(\frac{\partial G^n}{\partial y} - \frac{\Delta t}{\rho}\frac{\partial^2 \hat{p}}{\partial y^2}\Big) \tag{3.11}$$

Rearranging this expression to isolate the pressure terms, we achieve the Poisson equation which will be solved using the Conjugate Gradient method [10];

$$\delta^2\frac{1}{\rho}\frac{\partial^2 \hat{p}}{\partial x^2} + \frac{1}{\rho}\frac{\partial^2 \hat{p}}{\partial y^2} = \frac{1}{\Delta t}\Big(\delta\frac{\partial F^n}{\partial x} + \frac{\partial G^n}{\partial y}\Big) \tag{3.12}$$

Thus the general algorithm will be to compute F^n and G^n for a given timestep, then, solve for the pressure, P^{n+1}, at the next time step using the rearranged continuity equation above. Then we will compute the velocities, U^{n+1} and V^{n+1} for the next time step using the pressure and F^n and G^n terms. Finally, we will use these velocities to compute the advection of the level set function and the location of the new fluid interface, the details of which will be discussed later in this chapter.

3.3 Velocity Derivatives

We will now discuss the discretization of F^n and G^n. They have been rewritten here with their spatial indices replacing their temporal indices for clarity;

$$F_{i,j} = \delta u_{i,j} + \Delta t\Big(\frac{\delta^2}{Re}\Big[\frac{\partial^2 u}{\partial x^2}\Big]_{i,j} + \frac{1}{Re}\Big[\frac{\partial^2 u}{\partial y^2}\Big]_{i,j} - \delta\Big[\frac{\partial u^2}{\partial x}\Big]_{i,j} - \delta\Big[\frac{\partial uv}{\partial y}\Big]_{i,j}\Big), \tag{3.13}$$

$$G_{i,j} = \delta^2 v_{i,j} + \Delta t\Big(\frac{\delta^3}{Re}\Big[\frac{\partial^2 v}{\partial x^2}\Big]_{i,j} + \frac{\delta}{Re}\Big[\frac{\partial^2 v}{\partial y^2}\Big]_{i,j} - \delta^2\Big[\frac{\partial v^2}{\partial y}\Big]_{i,j} - \delta^2\Big[\frac{\partial uv}{\partial x}\Big]_{i,j} - \frac{g}{g'}\Big). \tag{3.14}$$

All terms here are computed for the nth time step and the velocity derivatives have been replaced with notation for their discrete approximations using square brackets. These terms are computed at the centre of the vertical cell boundary for the F terms and the horizontal cell boundaries for the G terms. As can be observed, we need to approximate four derivatives terms to compute F and G respectively.

3.3.1 Diffusive Terms

The diffusive terms in F and G; $[\frac{\partial^2 u}{\partial x^2}]$, $[\frac{\partial^2 u}{\partial y^2}]$, $[\frac{\partial^2 v}{\partial x^2}]$ and $[\frac{\partial^2 v}{\partial y^2}]$ within a single fluid are simply replaced with their full mesh length central difference approximations. An example for the $[\frac{\partial^2 u}{\partial x^2}]$ is given here;

$$\Big[\frac{\partial^2 u}{\partial x^2}\Big]_{i,j} = \frac{u_{i+1,j} - 2u_{i,j} + u_{i-1,j}}{\Delta x^2}. \tag{3.15}$$

However, the diffusive terms must be treated separately along the fluid interface due to differing densities of the two fluids. When the viscosity is not constant the full diffusive term must be expressed as follows;

$$\frac{\delta^2}{\mu Re}\frac{\partial}{\partial x}\Big(\mu\frac{\partial u}{\partial x}\Big). \tag{3.16}$$

Along the interface there are different μ's on each side of the boundary. We will numerically approximate the derivative near the interface as follows;

$$\Big[\mu\frac{\partial^2 u}{\partial x^2}\Big]_{i,j} = \frac{1}{\Delta x}\Big(\Big[\mu\frac{\partial u}{\partial x}\Big]_{i+\frac{1}{2},j} - \Big[\mu\frac{\partial u}{\partial x}\Big]_{i-\frac{1}{2},j}\Big). \tag{3.17}$$

Now suppose the interface crosses between points (i, j), which belongs to the first fluid, and $(i + 1, j)$, which belongs to the second fluid. This means that only the $[\mu\frac{\partial u}{\partial x}]_{i+\frac{1}{2},j}$ term will be affected by the change in viscosity. We can approximate this term across the boundary using the interface condition previously derived in the preceding chapter, restated here for convenience;

$$\mu_1\frac{\partial u}{\partial x} = \mu_2\frac{\partial u}{\partial x}. \tag{3.18}$$

Let u_I be the velocity at the interface between points (i, j) and $(i + 1, j)$ we can numerically approximate the interface condition. We do this by taking the finite difference approximation to the derivative between (i, j) and u_I as well as between u_I and $(i + 1, j)$;

$$\mu_2\frac{u_{i+1,j} - u_I}{\Delta x} = \mu_1\frac{u_I - u_{i,j}}{\Delta x}. \tag{3.19}$$

Using this relation we can isolate for u_I in terms of the velocities and viscosities on either side of the interface;

$$u_I = \frac{\mu_2 u_{i+1,j} + \mu_1 u_{i,j}}{\mu_1 + \mu_2}. \tag{3.20}$$

Using this expression for u_I we can approximate the $[\mu\frac{\partial u}{\partial x}]_{i+\frac{1}{2},j}$ term;

$$\Big[\mu\frac{\partial u}{\partial x}\Big]_{i+\frac{1}{2},j} = \mu_1\frac{u_I - u_{i,j}}{\theta\Delta x}, \tag{3.21}$$

where,

$$\theta = \frac{\frac{\phi_{i,j}+\phi_{i+1,j}}{2}}{\frac{\phi_{i,j}+\phi_{i+1,j}}{2} - \frac{\phi_{i+1,j}+\phi_{i+2,j}}{2}}. \tag{3.22}$$

In the above expression for θ, we use linear interpolation to centre the value of ϕ where the u values are centered. Then we compute θ which ranges from 0 to 1 and expresses where between points (i, j) and $(i+1, j)$ the interface is located. This process is analogous

between points (i,j) and $(i-1,j)$ or (i,j) and $(i,j+1)$, where θ always expresses the fraction of Δx or Δy that is between (i,j) and the interface. Previous approaches similar to this can be found in Gibou et al. [7] and Stewart [27]. While the denominator can be zero in theory, using an initial interface that is carefully chosen to be offset from the grid makes it very unlikely this will occur and this was not observed to occur in our simulations.

We can reexpress the approximation for the derivative in a more elegant way by introducing $\hat{\mu}$ which represents a weighted average of the viscosities at the boundary;

$$\Big[\mu\frac{\partial u}{\partial x}\Big]_{i+\frac{1}{2},j} = \frac{\mu_1\mu_2}{\hat{\mu}}\frac{u_{i+1,j}-u_{i,j}}{\Delta x}, \tag{3.23}$$

where,

$$\hat{\mu} = \mu_1\theta + \mu_2(1-\theta). \tag{3.24}$$

This process is analogous for the $[\mu\frac{\partial u}{\partial x}]_{i-\frac{1}{2},j}$ term and similar terms in the vertical dimension as well as terms within the expression for G.

3.3.2 Advective Terms

For the advective terms such as $[\frac{\partial(u^2)}{\partial x}]_{i,j}$, $[\frac{\partial(v^2)}{\partial y}]_{i,j}$, $[\frac{\partial(uv)}{\partial x}]_{i,j}$ and $[\frac{\partial(uv)}{\partial y}]_{i,j}$, a more complex approach is required. In order to increase stability at high Reynolds numbers, these terms will be computed using the central difference approximation mixed with the donor cell method [8]. We give the discretization for the $[\frac{\partial(u^2)}{\partial x}]_{i,j}$ and $[\frac{\partial(uv)}{\partial y}]_{i,j}$ terms here, centered at the right cell boundary;

$$\begin{aligned}\Big[\frac{\partial(u)^2}{\partial x}\Big]_{i,j} &= \frac{1}{\Delta x}\Big(\Big(\frac{u_{i,j}+u_{i+1,j}}{2}\Big)^2 - \Big(\frac{u_{i,j}+u_{i-1,j}}{2}\Big)^2\Big) \\ &+ \gamma\frac{1}{\Delta x}\Big(\Big(\frac{|u_{i,j}+u_{i+1,j}|(u_{i,j}+u_{i+1,j}\Big)}{4}\Big) - \Big(\frac{|u_{i,j}+u_{i-1,j}|(u_{i,j}+u_{i-1,j}\Big)}{4}\Big)\Big),\end{aligned} \tag{3.25}$$

$$\begin{aligned}\Big[\frac{\partial(uv)}{\partial y}\Big]_{i,j} &= \frac{1}{\Delta y}\Big(\Big(\frac{v_{i,j}+v_{i+1,j}}{2}\Big)\Big(\frac{u_{i,j}+u_{i,j+1}}{2}\Big) - \Big(\frac{v_{i,j-1}+v_{i+1,j-1}}{2}\Big)\Big(\frac{u_{i,j}+u_{i,j-1}}{2}\Big)\Big) \\ &+ \gamma\frac{1}{\Delta y}\Big(\Big(\frac{|v_{i,j}+v_{i+1,j}|(u_{i,j}+u_{i,j+1})}{4}\Big) - \Big(\frac{|v_{i,j-1}+v_{i+1,j-1}|(u_{i,j}+u_{i-1,j})}{4}\Big)\Big).\end{aligned} \tag{3.26}$$

The other terms are computed analogously but centered at the upper cell boundary. The γ parameter above determines the mixing between the central difference and donor cell methods. For all simulations within this work, this value was set to 0.9.

3.4 Solving the Poisson Equation for Pressure

In order to find the pressure at the next time step we need to construct an approximation to the Poisson equation, shown here;

$$\delta^2\Big[\frac{1}{\rho}\frac{\partial^2\hat{p}}{\partial x^2}\Big]_{i,j} + \Big[\frac{1}{\rho}\frac{\partial^2\hat{p}}{\partial y^2}\Big]_{i,j} = \frac{1}{\Delta t}\Big(\delta\Big[\frac{\partial F^n}{\partial x}\Big]_{i,j} + \Big[\frac{\partial G^n}{\partial y}\Big]_{i,j}\Big). \tag{3.27}$$

Our approximation will be centered at the cell centres, where pressure is computed.

For the right hand side of this equation, we will use central differencing of the F and G terms. Due to F and G being offset from the cell centres, where pressure values are computed, this amounts to forward differencing with respect to the natural indices of the F and G grids. We will refer to this right hand side as H, which has the same dimensions as the pressure grid and is also centred at the cell centres;

$$H_{i,j} = \frac{1}{\Delta t}\Big(\delta\Big[\frac{\partial F^n}{\partial x}\Big]_{i,j} + \Big[\frac{\partial G^n}{\partial y}\Big]_{i,j}\Big) = \frac{1}{\Delta t}\Big(\delta\frac{F_{i+1,j} - F_{i,j}}{\Delta x} + \frac{G_{i+1,j} - G_{i,j}}{\Delta y}\Big). \tag{3.28}$$

For the left hand side, we will discretize using standard central differencing when all points within the numerical stencil are within the same fluid;

$$\delta^2\Big[\frac{1}{\rho}\frac{\partial^2\hat{p}}{\partial x^2}\Big]_{i,j} + \Big[\frac{1}{\rho}\frac{\partial^2\hat{p}}{\partial y^2}\Big]_{i,j} = \delta^2\frac{1}{\rho}\frac{(\hat{p}_{i+1,j} - 2\hat{p}_{i,j} + \hat{p}_{i-1,j})}{\Delta x^2} + \frac{1}{\rho}\frac{(\hat{p}_{i,j+1} - 2\hat{p}_{i,j} + \hat{p}_{i,j-1})}{\Delta y^2}. \tag{3.29}$$

Note that in this case the density can be factored out of the derivative as it is constant within the same fluid.

When the pressure derivatives are taken across the interface however, we must treat it similarly to the diffusive velocity terms in the previous section, but in this case it is due to the differing densities. The single fluid case can also be expressed as follows;

$$\Big[\frac{1}{\rho}\frac{\partial^2\hat{p}}{\partial x^x}\Big]_{i,j} = \frac{\Big[\frac{1}{\rho}\frac{\partial\hat{p}}{\partial x}\Big]_{i+\frac{1}{2},j} - \Big[\frac{1}{\rho}\frac{\partial\hat{p}}{\partial x}\Big]_{i-\frac{1}{2},j}}{\Delta x}. \tag{3.30}$$

We can therefore use the interface condition given below to approximate the required terms, depending which is affected by the interface [5];

$$\frac{1}{\rho_1}\frac{\partial\hat{p}}{\partial x} = \frac{1}{\rho_2}\frac{\partial\hat{p}}{\partial x}. \tag{3.31}$$

Again let us assume that the fluid interface runs between points (i, j) and $(i+1, j)$. This implies the density will differ at each grid point. We can again imagine the pressure at the interface to be $\hat{p}_I$ and derive the following expression using central differencing;

$$\frac{1}{\rho_2}\frac{\hat{p}_{i+1,j} - \hat{p}_I}{\Delta x} = \frac{1}{\rho_1}\frac{\hat{p}_I - \hat{p}_{i,j}}{\Delta x}, \tag{3.32}$$

$$\hat{p}_I = \frac{\rho_2 \hat{p}_{i+1,j}\theta + \rho_1 \hat{p}_{i,j}(1-\theta)}{\rho_1\theta + \rho_2(1-\theta)}, \tag{3.33}$$

where,

$$\theta = \frac{\phi_{i,j}}{\phi_{i,j} - \phi_{i+1,j}}. \tag{3.34}$$

Again, while the denominator can be zero in theory, using an initial interface that is carefully chosen to be offset from the grid makes it very unlikely this will occur and this was not observed to occur in our simulations.

Now given the expression for the pressure at the interface we can use it to approximate the $[\frac{1}{\rho}\frac{\partial \hat{p}}{\partial x}]_{i+\frac{1}{2},j}$ term;

$$\Big[\frac{1}{\rho}\frac{\partial \hat{p}}{\partial x}\Big]_{i+\frac{1}{2},j} = \frac{1}{\rho_1}\frac{\hat{p}_I - \hat{p}_{i,j}}{\Delta x}. \tag{3.35}$$

Substituting for $\hat{p}_I$ and rearranging, we arrive at the following approximation;

$$\Big[\frac{1}{\rho}\frac{\partial \hat{p}}{\partial x}\Big]_{i+\frac{1}{2},j} = \frac{1}{\hat{\rho}}\frac{\hat{p}_{i+1,j} - \hat{p}_{i,j}}{\Delta x}, \tag{3.36}$$

where,

$$\hat{\rho} = \rho_1\theta + \rho_2(1-\theta). \tag{3.37}$$

The above reasoning also applies to the $[\frac{1}{\rho}\frac{\partial \hat{p}}{\partial x}]_{i-\frac{1}{2},j}$ term if the interface were to cross between (i, j) and $(i-1, j)$, along with those derivatives in the vertical direction. Thus, the full approximation for the $[\frac{1}{\rho}\frac{\partial^2 \hat{p}}{\partial x^2}]_{i,j}$ term can be expressed as follows;

$$\Big[\frac{1}{\rho}\frac{\partial^2 \hat{p}}{\partial x^2}\Big]_{i,j} = \frac{1}{\hat{\rho}}\frac{\hat{p}_{i+1,j} - \hat{p}_{i,j}}{\Delta x^2} - \frac{1}{\rho_2}\frac{\hat{p}_{i,j} - \hat{p}_{i-1,j}}{\Delta x^2}. \tag{3.38}$$

We can therefore derive a discrete approximation for pressure derivatives within, and on the boundary between, each fluid as well as for the right hand side derivatives of F and G. We also recall that we already know F and G when solving for pressure and thus can compute a fixed vector, H, for the right hand side. We can therefore express the Poisson equation as a linear system;

$$\mathbf{A}\hat{P} = H. \tag{3.39}$$

Where $\mathbf{A}$ is a multi-diagonal discretization matrix. We can therefore solve for the pressure values using any generic linear solver; for this work we use the Conjugate Gradient Method [10] because it is easy to modify to accommodate the interface conditions and the matrix is Positive Semi-Definite.

3.5 Computing the Velocity Update

Once the pressure has been computed for time $(n+1)$, we can use it to find the velocities u^{n+1} and v^{n+1} via the previously derived expressions, rewritten here in their discrete form;

$$u^{n+1} = \frac{F^n}{\delta} - \Delta t\Big[\frac{1}{\rho}\frac{\partial \hat{p}}{\partial x}\Big]_{i,j}, \tag{3.40}$$

$$v^{n+1} = \frac{1}{\delta^2}\Big(G^n - \Delta t\Big[\frac{1}{\rho}\frac{\partial \hat{p}}{\partial y}\Big]_{i,j}\Big). \tag{3.41}$$

We have already discussed how to compute F^n and G^n and how to solve for pressure. However, we must be careful with the discrete approximation for $[\frac{1}{\rho}\frac{\partial \hat{p}}{\partial x}]$ and $[\frac{1}{\rho}\frac{\partial \hat{p}}{\partial y}]$ along the interface as the density value will change. We will approximate these in the same way we did for the Poisson equation discretization, shown here;

$$\Big[\frac{1}{\rho}\frac{\partial \hat{p}}{\partial x}\Big]_{i,j} = \frac{1}{\hat{\rho}}\frac{\hat{p}_{i+1,j} - \hat{p}_{i,j}}{\Delta x}, \tag{3.42}$$

where,

$$\hat{\rho} = \rho_1\theta + \rho_2\theta, \tag{3.43}$$

and,

$$\theta = \frac{\phi_{i,j}}{\phi_{i,j} - \phi_{i+1,j}}. \tag{3.44}$$

When the points within the numerical stencils all lie within the same fluid, we use normal central differencing to approximate the terms.

3.6 Initializing and Advecting the Level Set Function

We choose the initial shape of the level set function so that its zero level set forms the desired starting interface for the gravity current problem. Furthermore, we desire a well behaved level set function which is smooth and has a slope of near 1 for increased numerical stability [5]. As the gravity current problem we are simulating requires a rectangular volume of denser fluid initially, we use the following formula to initialize the level set function;

$$\phi_{i,j} = max(|(i-1)\cdot\Delta x - x_0|, |(j-1)\cdot\Delta y - y_0|) - \frac{L}{2}. \tag{3.45}$$

The above expression describes an inverted pyramid in three dimensions. In the expression, x_0 and y_0 represent the location of the minimum point of the pyramid and L represents the length of the sides of the pyramid where it forms its zero level set. We centre the pyramid outside of our domain so that only two sides transit through it. Figure 3.2 shows ϕ defined over the domain at the start of the simulation.

Once the velocity field for time step $(n+1)$ is computed, we must advect the fluid interface under these new conditions. From the formulation of the level set method discussed in the previous chapter we have the following expression to work from;

$$\frac{\partial\phi}{\partial t} + \vec{u}\cdot\nabla\phi = 0, \tag{3.46}$$

which can be approximated,

$$\phi^{n+1} = \phi^n - \Delta t(\phi_x u + \phi_y v). \tag{3.47}$$

The reader may recognize the above as a conservation law. We use the Minmod Flux Limiting Scheme with Lie dimension splitting to achieve second order spatial accuracy in approximating the time stepping of the level set. More details on this scheme can be found in the associated reference [19].

3.7 Boundary Conditions

In order to implement the above discretizations we must implement the boundary conditions for the velocity fields, the pressure and the level set function. We begin with the

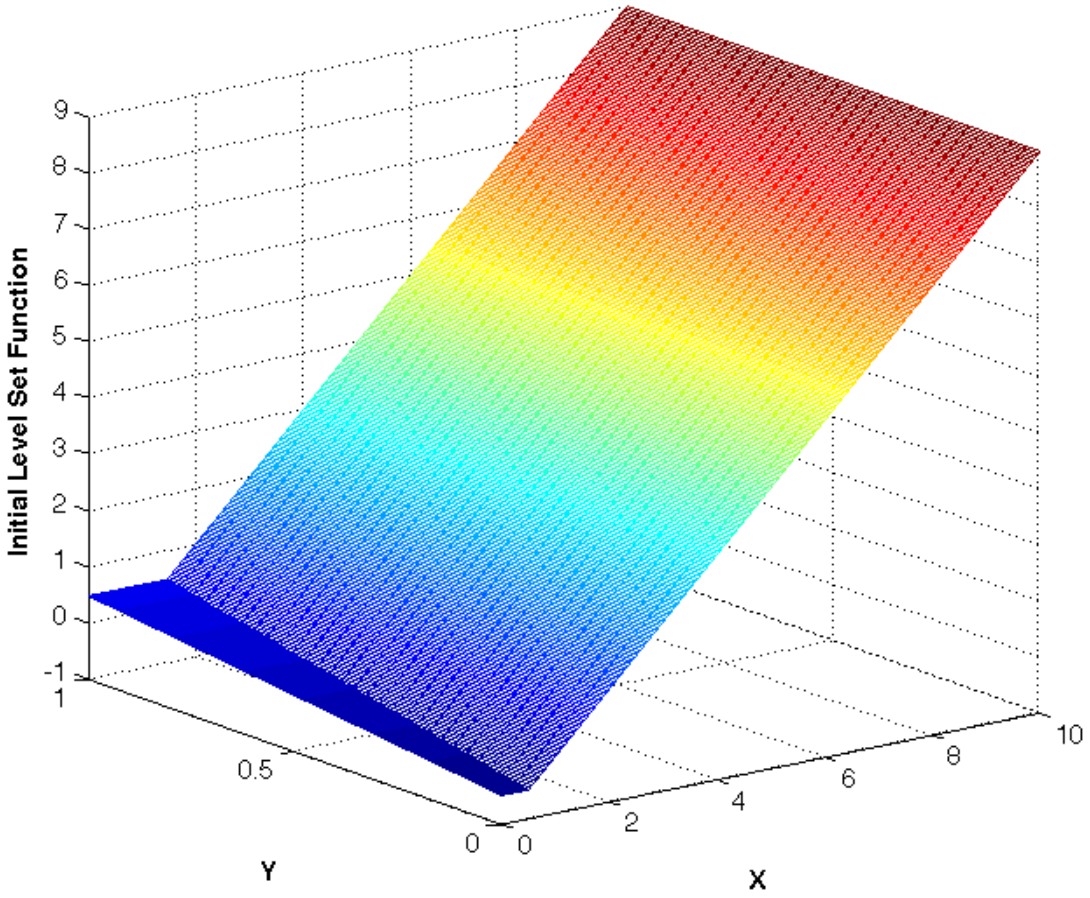

Figure 3.2: *This figure shows the initial ϕ configuration.*

velocity fields; we have no-slip, solid boundaries with the following conditions at the left and bottom borders of the domain, and their implied numerical constraints;

Bottom boundary:

$$v = 0,\ \frac{\partial u}{\partial y} = 0 \implies v_{i,0} = 0,\ u_{i,0} = u_{i,1}, \tag{3.48}$$

Left boundary:

$$u = 0,\ \frac{\partial v}{\partial x} = 0 \implies u_{0,j} = 0,\ v_{0,j} = v_{1,j}. \tag{3.49}$$

These conditions imply that the perpendicular velocities go to zero at the border and that the velocities moving parallel to the boundary have zero gradient in the direction perpendicular to it.

The top and right boundary will impose a free slip, outflow conditions on the velocity fields. To enforce these conditions we have the following constraints and implications;

Top boundary:

$$\frac{\partial u}{\partial y} = 0,\ \frac{\partial v}{\partial y} = 0 \implies u_{i,j_{max}} = u_{i,j_{max}-1},\ v_{i,j_{max}} = v_{i,j_{max}-1}, \tag{3.50}$$

Right boundary:

$$\frac{\partial v}{\partial x} = 0,\ \frac{\partial u}{\partial x} = 0 \implies v_{i_{max},j} = v_{i_{max}-1,j},\ u_{i_{max},j} = u_{i_{max}-1,j}. \tag{3.51}$$

For the pressure solver we impose Neumann type boundary conditions. This has the following implications for our discretization;

Left and right boundaries:

$$\frac{\partial \hat{p}}{\partial x} = 0 \implies \hat{p}_{i,0} = \hat{p}_{i,1},\ \hat{p}_{i,j_{max}} = \hat{p}_{i,j_{max}-1}, \tag{3.52}$$

Top and bottom boundaries:

$$\frac{\partial \hat{p}}{\partial y} = 0 \implies \hat{p}_{0,j} = \hat{p}_{1,j},\ \hat{p}_{i_{max},j} = \hat{p}_{i_{max}-1,j}. \tag{3.53}$$

The above defines the numerical implementation of the boundary conditions on the pressure and velocity fields, however we compute the F and G terms as a step in the computation. We will also need to derive boundary conditions consistent with the above for these quantities. Specifically we will need boundary conditions for the right and left borders of F and the top and bottom borders of G due to the derivative terms used to

compute H. From our discretized and rearranged velocity update formula we observe the following at the left and bottom borders;

$$\frac{\hat{p}_{0,j}^{n+1} - \hat{p}_{1,j}^{n+1}}{\Delta x} = \frac{1}{\Delta t}\Big(u_{0,j}^{n+1} - \frac{F_{0,j}^{n}}{\delta}\Big), \tag{3.54}$$

$$\frac{\hat{p}_{i,0}^{n+1} - \hat{p}_{i,1}^{n+1}}{\Delta y} = \frac{1}{\Delta t}\Big(G_{i,0}^{n} - \delta^2 v_{i,0}^{n+1}\Big). \tag{3.55}$$

In order to be consistent with the Neumann boundary condition for pressure we require that right hand side of both equations be zero implying the following constraints, and by symmetry we also arrive at analogous constraints for the top and right boundaries;

$$F_{0,j}^{n} = \delta\ u_{0,j}^{n+1}, \quad F_{i_{max},j}^{n} = \delta\ u_{i_{max},j}^{n+1}, \tag{3.56}$$

$$G_{i,0}^{n} = \delta^2\ v_{i,0}^{n+1} \quad G_{i,j_{max}}^{n} = \delta^2\ v_{i,j_{max}}^{n+1}. \tag{3.57}$$

Finally, the level set function needs appropriate boundaries to enforce proper interaction between the interface and the boundaries. We enforce the following conditions along the boundaries, and their numerical implications;

Left and right boundaries:

$$\frac{\partial \phi}{\partial x} = 0 \implies \phi_{i,0} = \phi_{i,1},\ \phi_{i,j_{max}} = \phi_{i,j_{max}-1}, \tag{3.58}$$

Top and bottom boundaries:

$$\frac{\partial \phi}{\partial y} = 0 \implies \phi_{0,j} = \phi_{1,j},\ \phi_{i_{max},j} = \phi_{i_{max}-1,j}. \tag{3.59}$$

3.8 Variable Timestepping and Stability Conditions

As previously stated we use explicit, variable time stepping to compute the solution to the gravity current problem. We start the simulation with a step size of 0.02 and adjust the step size in order to preserve stability. The stability conditions are derived from the advection terms in the momentum equation, in each dimension, and their associated Courant-Friedrichs-Lewy Condition (CFL), as well as the diffusive constant associated with the diffusion terms. The three resulting conditions are given here;

$$\Delta t < \frac{\Delta x}{|u_{max}|}, \quad \Delta t < \frac{\Delta y}{|v_{max}|}, \quad \Delta t < \frac{\min(Re_1, Re_2)}{2}\Big(\frac{1}{\frac{1}{\Delta x^2} + \frac{1}{\Delta y^2}}\Big). \tag{3.60}$$

Observe that the third condition depends on the Reynolds number due to the fact that the rate of diffusion depends on this value. Therefore, as there are two fluids involved in the simulation, with two different Reynolds numbers, this condition is actually two separate conditions. Using these conditions and a safety factor τ, we construct the equation for the time step size update;

$$\Delta t = \tau \cdot \min\Big(\frac{\Delta x}{|u_{max}|}, \frac{\Delta y}{|v_{max}|}, \frac{\min(Re_1, Re_2)}{2}\Big(\frac{1}{\frac{1}{\Delta x^2} + \frac{1}{\Delta y^2}}\Big)\Big). \tag{3.61}$$

The observant reader may note that the advection of the level set method also imposes its own stability conditions, however as the level set method advects with a velocity equal to that of the surrounding fluid, the resulting conditions are identical to the CFL conditions listed above.

3.9 Algorithm Summary

Finally we are able to state clearly the steps of the algorithm for the discrete approximation of the gravity current problem. The steps are enumerated below.

Algorithm 1 Level Set Fluid Interface Simulation Algorithm

1: Initialize parameters, set t=0.
2: Initialize velocity and pressure fields to 0, initialize level set as described.
3: Enforce boundary conditions on each grid; U, V, P and ϕ.
4: **while** While $t < T_{final}$: **do**
5: Update the time step if required.
6: Compute F^n and G^n.
7: Compute H^n.
8: Solve the Poisson equation for pressure.
9: Compute U^n and V^n.
10: Enforce boundary conditions on U and V.
11: **end while**

Chapter 4

Results and Discussion

In this chapter we will present the findings from our numerical experiments and compare them to past works, specifically that of D'Alessio et al.[2]. We start by explaining the procedure used to select various parameters used for our simulation, including the grid and domain size, as well as the tolerance for the Conjugate Gradient solver. We will then present the results of the numerical simulation by comparing the location of the fluid boundary for increasing Reynolds numbers. We will compare these results to previous numerical work solving the inviscid case in order to asses the viability of our numerical approach.

4.1 Experiments to Select the Simulation Parameters

Before running the numerical simulations and comparing to the results, it is first necessary to ensure that appropriate parameters are selected to achieve the required accuracy and create conditions that closely emulate the physical system being investigated. The parameters requiring investigation include grid spacing, domain size, boundary conditions and the tolerance for the linear solver. This procedure is not exact and requires some qualitative judgment and experience with the physical phenomena. The final parameter settings can be seen in Table 4.2 at the end of this section.

4.1.1 Selecting the Grid Spacing

We begin with grid spacing, which is important because the fineness of the grid directly influences the spatial accuracy of the algorithm, and thus our ability to locate the fluid interface. Grid spacing, due to its relation to spatial accuracy, affects the conservation of mass between the two fluids. Accumulating errors in the boundary location will change the ratio of the two fluid volumes. However, it is also important to note that excessive refinement of the grid size will result in higher computational costs and runtimes. Thus we aim for an appropriate compromise given experimental constraints.

In order to select the grid size we performed two different experiments. First we simulated the fluid flow for various grid sizes and qualitatively compare the location of the interface. The ideal grid spacing should be fine enough such that any further refinement has a marginal effect on the interface location. We found a spacing of at least 0.0125 was reasonable to meet this requirement given the computational constraints. A comparison of the interface location for different grid spacings can be seen in Figure 4.1.

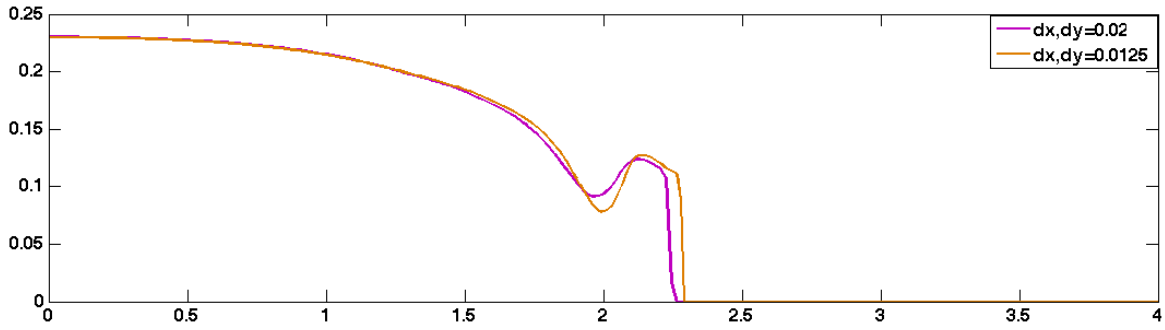

Figure 4.1: *This figure compares the interface location at a final time of 3, for a grid spacing of 0.02 and 0.0125. There is little qualitative variation in the interface location, and only a small difference in the location of the leading edge.*

Secondly, we specifically investigated the grid spacing's effect on the level set advection scheme accuracy and the conservation of mass. In order to do this we ran the level set advection scheme for fixed velocity fields. We thus did not use the full Navier Stokes solver, but rather the level set advection step alone to advance the interface in time within a fixed solenoidal velocity field. We did this for a range of grid spacings, velocity fields and initial conditions and also compared upwinding and the Minmod Flux Limiting scheme. At the final time we compared initial volume of the denser fluid to the final volume in order to

access the level of conservation achieved. We found that the ideal grid spacing may be as fine as 0.0025, however this spacing would be too costly to simulate in the time available. We therefore accepted fairly reasonable results at 0.01. An example of the results for these experiments can be seen in Table 4.1, where we used a fixed velocity field, computed using the Navier Stokes solver, for the first time step, to advect the level set until a time of 3 for different grid sizes.

Table 4.1: *A table showing the percentage volume loss of the denser fluid advected through a fixed velocity field until a final time of 3.*

Parameter	**Value**
Grid Spacing	Percentage Loss
0.01	2.292%
0.005	0.415%
0.0025	0.108%
0.00125	0.0292%

4.1.2 Selecting the Domain Size and Boundary Conditions

The physical system being simulated by our numerical algorithm is one where the top and right boundaries of the domain should be far enough away that they have minimal effect on the gravity current interface. In the ideal case the domain would be unbounded in these directions but this is not computationally feasible. We attempt to emulate this in two ways, firstly, by selecting appropriate boundary conditions and secondly, by selecting a domain size large enough that the fluid interface remains comparatively far from the top and right boundaries.

We first compared boundary conditions on the top and right boundaries. We ran simulations with impermeable boundaries with a free-slip condition on all walls. We found this caused a vortex to form within the domain due to the inability for fluid at the top and right boundaries to flow out of the domain. We then implemented the outflow conditions described in the previous two chapters which did not produce vortices and more closely emulated the desired physical conditions as it allowed free movement of the fluid in and out of the simulated region. The solid boundaries also resulted in different propagation speeds compared with the outflow conditions, with the solid boundaries resulting in slower speeds. We therefore chose to use the outflow conditions for the top and right boundary. A sample of the experimental results can be seen in Figure 4.2.

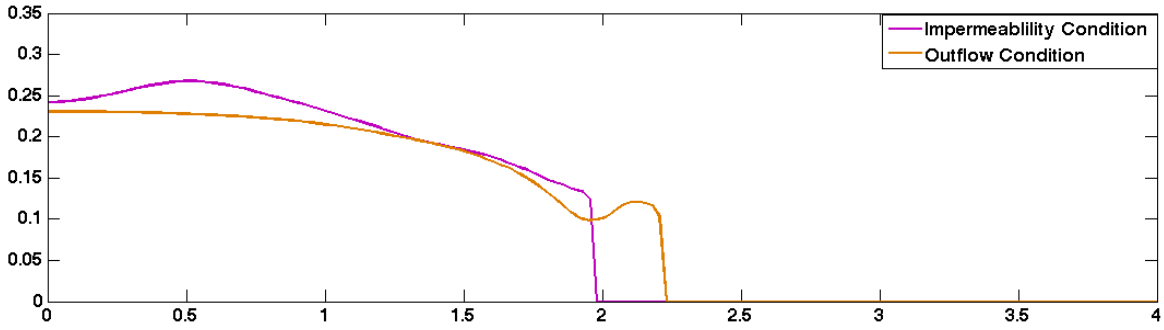

Figure 4.2: *A visualization of the fluid interface location for the outflow boundary condition in blue and the solid boundary condition in red ,simulated until a final time of 3. It can clearly be seen that the solid boundaries cause a slower propagation of the gravity current.*

We then enlarged the domain by 50%, from the 1 by 10 size we used during earlier tests, to investigate the qualitative effect of domain size on the interface shape and its propagation speed. We found slight variations in the interface height but almost no difference in propagation speed by a final time of 3. We thus concluded that a 1 by 10 domain size was sufficient for our purposes. A comparison of interface locations at a time of 3 can be seen in Figure 4.3 for the two different domain sizes.

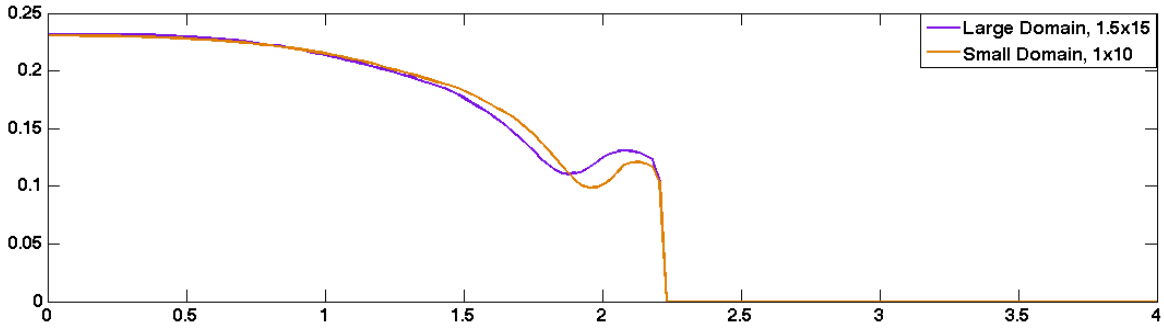

Figure 4.3: *A visualization of the fluid interface location for the larger domain,* 1.5×15*, in purple and the smaller domain,* 1×10*, in orange ,simulated until a final time of 3. It can be seen that while there is some small variation in the interface height, the propagation speed of the current is not significantly affected.*

4.1.3 Selecting the Tolerance for the Conjugate Gradient Method

The Conjugate Gradient method, used to solve for the pressure, is an iterative algorithm and therefore requires a tolerance to be specified for its stopping criterion. We would ideally like as accurate a pressure solution as possible, however the pressure solver is the most computationally expensive part of the overall algorithm and thus decreasing the tolerance can greatly decrease the runtime of each simulation. Furthermore, the accuracy of the pressure solution is bounded by the spatial and temporal accuracies achieved by the other approximations in the algorithm. Knowing pressure to decimal places beyond this value is not necessary as it will not increase the precision of the computed fluid interface.

We have run a number of simulations varying the tolerance from 1e-07 down to 1e-04, visualizing the fluid interface side-by-side in each case. We found that we achieved almost no variation in the interface location with a tolerance as low as 1e-04, and achieved a significant decrease in runtime as a result. In fact, it was not possible to distinguish the interface locations from each other when they were graphed due to their overlap. We therefore chose a tolerance of 1e-04.

Table 4.2: *A table specifying the parameter values for the simulations in this work.*

Parameter	**Value**
Domain Size	1x10
Initial Dam Dimensions [1]	0.5x1.0
Grid Spacing	0.01
CG Tolerance	1e-04
$\rho_1,\ \rho_2$	1.0, 0.9
$\mu_1,\ \mu_2$	1.0, 1.0
δ	0.1
$\frac{g}{g'}$	10

4.2 Comparison with the Inviscid Solution

We now present the results of our simulation in comparison to the work of D'Alessio et al.[2] which solved the inviscid case. We wish to assess whether our simulation results,

[1] This specifies the initial dimensions of the rectangular volume of denser fluid located at the bottom left of the domain at T=0.

specifically the fluid interface location, approaches those of the inviscid solution. The inviscid solution is for the case where inertial forces completely dominate viscous forces, and therefore the Reynolds numbers are effectively infinite. We wish to assess how our solution asymptotically approaches this special case as we increase the Reynolds numbers. We will pay specific attention to the propagation speed of the flow, meaning the horizontal rate at which the leading edge of the fluid moves across the domain.

To visualize these results we plot the interface location for Reynolds number pairings of (1000,900), (100000,90000) and (1000000,900000) against the inviscid solution at a time final time of 3. This comparison can be seen in Figure 4.4.

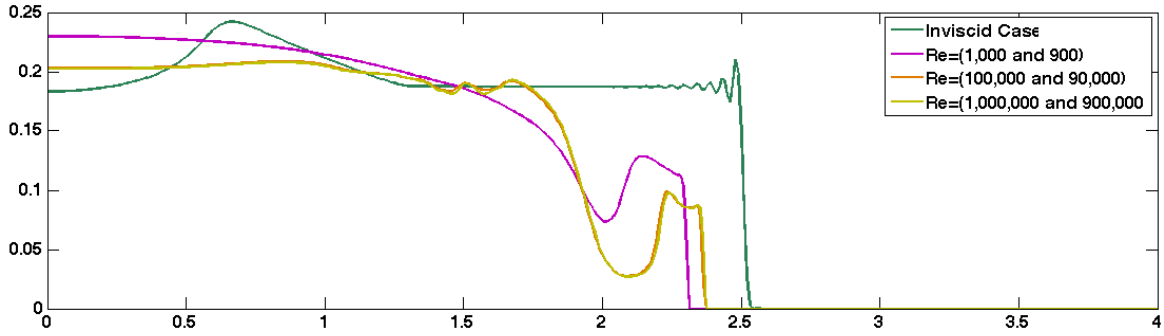

Figure 4.4: *A comparison of the numerical solution at three different Reynolds numbers against the inviscid results. The (1000000,900000) and (100000,90000) cases overlap significantly.*

It can be seen in Figure 4.4 that there are some significant differences in the shape of the fluid interface in all cases. It should be noted that the oscillations in the inviscid case are not physical and are due to Gibbs phenomenon. Our solutions generally have similar shaped interfaces, especially around the leading edge of the gravity current. However, as inertial forces are increased relative to their viscous counterparts, the gravity current begins to propagate at a higher speed. This results in the leading edges being offset from each other in each numerical simulation, those with larger Reynolds numbers having moved further by the end of the simulation. We can see that as the Reynolds number gets larger, the leading edge of the current gets closer to the inviscid solution.

However, we should also note that there is volume loss occurring in these simulations at a greater rate than experiments with the fixed velocity fields suggested, especially at higher Reynolds numbers. Numerical dissipation has been a major concern for maintaining

conservation as the level set function is advected. Although we used a second order scheme for the level set advection, higher order schemes would be a good topic for future work.

Chapter 5

Conclusion

In this work we have created a numerical algorithm for simulating a two-phase gravity current problem resulting from a dam break. Gravity currents have been of mathematical interest for over a century and we compare our numerical results to previous numerical work on an inviscid approximation. We have used the level set method to track the fluid interface in time and can compare the interface location and its rate of propagation against the previous work of D'Alessio et al. [2]. Our results suggest some reasonable agreement with the previous work. While the interface shape is clearly significantly affected by viscous forces, the rate of propagation of the gravity current's leading edge approaches the inviscid case at larger Reynolds numbers, as expected.

Conservation of mass and the resulting requirement of very fine grid spacing were a major concern in this work. Due to our desire to simulate the flow to large time values, very fine meshes were ideal in order to avoid excessive volume loss and avoid the accumulation of errors over long simulation runs. We used higher order schemes to advect the level set function with some success but nonconservation is still a major concern and a possible area of future investigation. Due to the finer mesh sizes and thus larger grids, replacing the Conjugate Gradient solver may also be of interest. The linear solver is the most computationally demanding part of the algorithm and is sensitive to increased grid sizes. Better methods exist, that scale more slowly with respect to grid size, however implementing the interface conditions in these methods is much more involved. However, this may be of interest in future work.

In this work we compared our numerical results to previous work for the inviscid case. In addition to this, there is also exists work on similarity solutions for highly viscous flows at very low Reynolds numbers. It would be interesting to assess our algorithm asymptotically

against these results as well.

Two-phase flows, and gravity currents in particular, will continue to be of interest due to their common occurrence in the nature and industry. Thus being able to construct accurate numerical simulations of these problems and validate them against theoretical results will continue to be of importance for years to come.

References

[1] TB Benjamin. Gravity currents and related phenomena. *Journal of Fluid Mechanics*, 31(02):209–248, 1968.

[2] SJD D'Alessio, TB Moodie, JP Pascal, and GE Swaters. Gravity currents produced by sudden release of a fixed volume of heavy fluid. *Studies in Applied Mathematics*, 96(4):359–385, 1996.

[3] BJ Daly and WE Pracht. Numerical study of density-current surges. *Physics of Fluids (1958-1988)*, 11(1):15–30, 1968.

[4] AJC Barre de Saint-Venant. Theorie du mouvement non permanent des eaux, avec application aux crues des rivieres eta l'introduction des mare es dans leurs lits. *Comptes Rendus des seances de l'Academie des Sciences*, 73:237–240, 1871.

[5] M Fattori. *A Level Set and Sharp Interface Approach for Simulating Incompressible Two-Phase Flow*. PhD thesis, University of Waterloo, 2014.

[6] M Felix. Flow structure of turbidity currents. *Sedimentology*, 49(3):397–419, 2002.

[7] F Gibou, RP Fedkiw, LT Cheng, and M Kang. A second-order-accurate symmetric discretization of the poisson equation on irregular domains. *Journal of Computational Physics*, 176(1):205–227, 2002.

[8] M Griebel, T Dornseifer, and T Neunhoeffer. *Numerical simulation in fluid dynamics: a practical introduction*, volume 3. Siam, 1997.

[9] RW Griffiths. Gravity currents in rotating systems. *Annual Review of Fluid Mechanics*, 18(1):59–89, 1986.

[10] MR Hestenes and E Stiefel. *Methods of conjugate gradients for solving linear systems*, volume 49. NBS, 1952.

[11] HE Huppert. The propagation of two-dimensional and axisymmetric viscous gravity currents over a rigid horizontal surface. *Journal of Fluid Mechanics*, 121:43–58, 1982.

[12] HE Huppert. Gravity currents: a personal perspective. *Journal of Fluid Mechanics*, 554:299–322, 2006.

[13] HE Huppert and JE Simpson. The slumping of gravity currents. *Journal of Fluid Mechanics*, 99(04):785–799, 1980.

[14] JM Hyman. Numerical methods for tracking interfaces. *Physica D: Nonlinear Phenomena*, 12(1):396–407, 1984.

[15] M Kang, RP Fedkiw, and XD Liu. A boundary condition capturing method for multiphase incompressible flow. *Journal of Scientific Computing*, 15(3):323–360, 2000.

[16] TW Kao, C Park, and HP Pao. Inflows, density currents, and fronts. *Physics of Fluids (1958-1988)*, 21(11):1912–1922, 1978.

[17] GH Keulegan. An experimental study of the motion of saline water from locks into fresh water channels. *Nat. Bur. Stand. Rept. Technical Report*, 5168, 1957.

[18] GH Keulegan. *Twelfth progress report on model laws for density currents: The motion of saline fronts in still water*, volume 5831. US Dept. of Commerce, National Bureau of Standards, 1958.

[19] D Kuzmin. On the design of general-purpose flux limiters for finite element schemes. i. scalar convection. *Journal of Computational Physics*, 219(2):513–531, 2006.

[20] E Maitre. Review of numerical methods for free interfaces. *Les Houches*, 27:31, 2006.

[21] GV Middleton. Experiments on density and turbidity currents: Iii. deposition of sediment. *Canadian Journal of Earth Sciences*, 4(3):475–505, 1967.

[22] AA Nepomnyashchy, MG Velarde, and P Colinet. *Interfacial phenomena and convection*. CRC Press, 2001.

[23] S Osher and R Fedkiw. *Level set methods and dynamic implicit surfaces*, volume 153. Springer Science & Business Media, 2006.

[24] JW Rottman and JE Simpson. Gravity currents produced by instantaneous releases of a heavy fluid in a rectangular channel. *Journal of Fluid Mechanics*, 135:95–110, 1983.

[25] JA Sethian. *Level set methods and fast marching methods: evolving interfaces in computational geometry, fluid mechanics, computer vision, and materials science*, volume 3. Cambridge Univ Press, 1999.

[26] JE Simpson. *Gravity currents: In the environment and the laboratory*. Cambridge Univ Press, 1997.

[27] PA Stewart, N Lay, M Sussman, and M Ohta. An improved sharp interface method for viscoelastic and viscous two-phase flows. *Journal of Scientific Computing*, 35(1):43–61, 2008.

[28] M Ungarish. *An introduction to gravity currents and intrusions*. CRC Press, 2009.

[29] M Ungarish. Two-layer shallow-water dam-break solutions for gravity currents in non-rectangular cross-area channels. *Journal of Fluid Mechanics*, 732:537–570, 2013.

[30] T Von Karman. The engineer grapples with nonlinear problems. *Bulletin of the American Mathematical Society*, 46(8):615–683, 1940.